

1 **Evaluation of high-resolution predictions of fine**
2 **particulate matter and its composition in an urban area**
3 **using PMCAMx-v2.0**
4

5 Brian T. Dinkelacker¹, Pablo Garcia Rivera¹, Ioannis Kioutsioukis², Peter J. Adams^{3,4},
6 Spyros N. Pandis^{5,6}

7
8 ¹*Department of Chemical Engineering, Carnegie Mellon University, Pittsburgh, PA,*
9 *15213*

10 ²*Department of Physics, University of Patras, 26500, Patras, Greece*

11 ³*Department of Civil and Environmental Engineering, Carnegie Mellon University,*
12 *Pittsburgh, PA, 15213*

13 ⁴*Department of Engineering and Public Policy, Carnegie Mellon University, Pittsburgh,*
14 *PA, 15213*

15 ⁵*Institute of Chemical Engineering Sciences (FORTH/ICE-HT), 26504, Patras, Greece*

16 ⁶*Department of Chemical Engineering, University of Patras, 26500, Patras, Greece*

17 *Correspondence to: Spyros N. Pandis (spyros@chemeng.upatras.gr)

18
19 **Abstract**

20 Accurately predicting urban PM_{2.5} concentrations and composition has proved challenging
21 in the past, partially due to the resolution limitations of computationally intensive chemical
22 transport models (CTMs). Increasing the resolution of PM_{2.5} predictions is desired to
23 support emissions control policy development and address issues related to environmental
24 justice. A nested grid approach using the CTM PMCAMx-v2.0 was used to predict PM_{2.5}
25 at increasing resolutions of 36 x 36, 12 x 12, 4 x 4, and 1 x 1 km for a domain largely
26 consisting of Allegheny County and the city of Pittsburgh in southwestern Pennsylvania,
27 US during February and July 2017. Performance of the model in reproducing PM_{2.5}
28 concentrations and composition was evaluated at the finest scale using measurements from
29 regulatory sites as well as a network of low-cost monitors. Novel surrogates were
30 developed to allocate emissions from cooking and on-road traffic sources to the 1 x 1 km
31 resolution grid. Total PM_{2.5} mass is reproduced well by the model during the winter period
32 with low fractional error (0.3) and fractional bias (+0.05) when compared to regulatory
33 measurements. Comparison with speciated measurements during this period identified
34 small underpredictions of PM_{2.5} sulfate, elemental carbon (EC), and organic aerosol (OA)
35 offset by a larger overprediction of PM_{2.5} nitrate (~~bias = +1.4 μg m⁻³, fractional bias =~~
36 ~~+0.81~~). In the summer period, total PM_{2.5} mass is underpredicted due to a large

Commented [BD1]: Referee #2 - Comment 6

37 underprediction of OA (bias = $-1.9 \mu\text{g m}^{-3}$, fractional bias = -0.41). ~~with fractional bias of~~
38 ~~0.39. Here, PM_{2.5}-nitrate is overpredicted again with a large fractional bias (+0.7) but~~
39 ~~significantly lower magnitude ($+0.4 \mu\text{g m}^{-3}$). Underpredictions in PM_{2.5}-sulfate and EC~~
40 ~~contribute to the negative prediction bias of total PM_{2.5} ($-0.4 \mu\text{g m}^{-3}$ and $-0.2 \mu\text{g m}^{-3}$,~~
41 ~~respectively), however the largest underprediction is seen for summer OA (bias = $-1.9 \mu\text{g}$~~
42 ~~m^{-3} , fractional bias = -0.41). In the winter period, the model performs well reproducing the~~
43 ~~variability between urban measurements and rural measurements of local pollutants such~~
44 ~~as EC and OA. This effect is less consistent in the summer period due to a larger fraction~~
45 ~~of long range transport OA. This effect is also captured well in the summer for EC,~~
46 ~~although the OA performance here is less consistent because much more of this OA is~~
47 ~~secondary and transported from outside of the inner modeling domain. Comparison with~~
48 ~~total PM_{2.5} concentration measurements from low-cost sensors showed improvements in~~
49 ~~performance with increasing resolution yielded similar results with slightly higher~~
50 ~~overpredictions seen in the winter (fractional bias = $+0.24$) and lower underpredictions~~
51 ~~seen in the summer (fractional bias = -0.27). Inconsistencies in PM_{2.5} nitrate predictions in~~
52 ~~both periods are believed to be due to errors in partitioning between PM_{2.5} and PM₁₀ modes~~
53 ~~and motivate improvements to the treatment of dust particles within the model. The~~
54 ~~underprediction of summer OA would likely be improved by updates to biogenic SOA~~
55 ~~chemistry within the model, which would result in an increase of long-range transport SOA~~
56 ~~seen in the inner modeling domain. These improvements are obvious topics for future work~~
57 ~~towards model improvement. Comparison with regulatory monitors showed that increasing~~
58 ~~resolution from 36 km to 1 km improved both fractional error and fractional bias in both~~
59 ~~modeling periods. by 0.04 in February 2017. In July 2017, fractional error decreased by~~
60 ~~0.05 and fractional bias improved by 0.07 with increasing resolution. Improvements at all~~
61 ~~types of measurement locations indicated an improved ability of the model to reproduce~~
62 ~~urban-rural PM_{2.5} gradients at higher resolutions.~~

64 1 Introduction

65 Fine particulate matter with aerodynamic diameter less than $2.5 \mu\text{m}$ (PM_{2.5}) has
66 been associated with public health concerns due to short and long-term exposure. Some of
67 the health effects of PM_{2.5} include increased risk of heart disease, increased likelihood of

Commented [BD2]: Referee #1 - Comment 3

68 heart attacks and strokes, impaired lung development, and increased risk of lung disease
69 (Dockery and Pope, 1994). Chemical transport models are frequently used for supporting
70 the development of air quality policies designed to protect public health. To evaluate these
71 policies, CTMs must simulate PM_{2.5} concentrations and their response to changes in
72 emissions accurately.

73 Grid resolution is an important factor for CTM studies focusing on major urban
74 areas since on-road traffic, commercial cooking, and biomass burning can have sharp
75 gradients at the urban scale (Lanz et al., 2007; Allan et al., 2010). High spatial resolution
76 measurements of PM₁ in the city of Pittsburgh in high source-impact locations are on
77 average 40% higher than at urban background locations (Gu et al., 2018). Heightened
78 organic aerosol concentrations have been observed in commercial districts containing
79 multiple restaurants (Robinson et al., 2018). The demographic characteristics of the
80 population can also have large variations at the neighborhood scale. High resolution
81 predictions of pollutant concentrations allow for exposure assessments that compare
82 subpopulations within the same metropolitan area to answer environmental justice related
83 questions (Anand, 2002). The benefits of high-resolution modeling must be balanced with
84 the increased complexity in the development of accurate, high-resolution emission
85 inventories and increased computational cost and storage requirements.

86 Previous studies have found small to modest improvements on the predictive ability
87 of regional CTMs for ozone in the summers of 1995, 1996, and 1997 moving from 36 km
88 to 12 km resolution (Arunachalam et al., 2006) as well as in July 1988 using a dynamic
89 grid system with sizes varying from 18.5 km to 4.625 km (Kumar and Russell, 1996).
90 Stroud et al. (2011) found that the accurate simulation of urban and large industrial plumes
91 required a grid resolution of 2.5 km in order to properly capture contributions from local
92 sources of primary organic aerosol (POA) and volatile organic compounds (VOCs).
93 Zakoura and Pandis (2019) investigated the effect of increasing grid resolution on PM_{2.5}
94 nitrate predictions and found that increasing the resolution to 4 km reduced bias by 65%.
95 Fountoukis et al. (2013) reported a reduction of the bias for black carbon (BC)
96 concentrations in the northeastern US when the grid resolution was reduced from 36x36
97 km to 4x4 km. Pan et al., (2017) allocated county-based emissions at 4 km and 1 km grid
98 resolution using the default approach from the National Emissions Inventory and found

99 small changes in model performance for NO_x and ozone. The 1 km simulation was able to
100 resolve the detailed spatial variability of emissions in heavily polluted areas including
101 highways, airports and industrially focused sub-regions.

102 One of the weaknesses of several of the above studies has been that the gridded
103 emissions used at the higher resolutions were the results of interpolation. It is not clear if
104 the remaining discrepancies between model predictions and measurements were due to
105 errors in the spatial distribution of the high-resolution emissions, errors in the overall
106 magnitude of the emissions over an urban area or other modeling errors in the simulation
107 of various processes (chemistry, condensation/evaporation, etc.). It is also not clear if errors
108 in previous simulations of urban PM_{2.5} are due to inaccuracies in the transport of regional
109 PM_{2.5} to urban areas. In this work, we explore the impacts of increasing the resolution of
110 emissions inputs and CTM output on PM_{2.5} predictions in southwestern Pennsylvania
111 during the months of February and July 2017, including the ability of the model to
112 reproduce observed differences between urban and rural PM_{2.5} at the various grid
113 resolutions.

114 Garcia Rivera et al. (2022) investigated the effects of increasing grid resolution of
115 model inputs and CTM output on source resolved predictions of PM_{2.5} concentration and
116 population exposure at 36 km, 12 km, 4 km, and 1 km. Moving to 12 x 12 km resolution
117 resolved much of the urban-rural gradient. Increasing to 4 x 4 km resolved stationary
118 sources such as power plants and the 1 x 1 km resolution results revealed intra-urban
119 variations and individual roadways. Regional pollutants with low spatial variability such
120 as PM_{2.5} nitrate showed modest changes when increasing the resolution to 4 x 4 km and
121 higher. Local pollutants such as black carbon and organic aerosol showed gradients that
122 were only resolved at the finest resolution. The ability of these simulations to reproduce
123 PM_{2.5} concentrations at different resolutions is evaluated here against multiple
124 measurement sources and types. Garcia Rivera et al. (2022) did not address model
125 performance and the corresponding challenges related to the different types of the available
126 measurements. The two months of February and July 2017 were chosen to maximize the
127 information gained with regards to the effects of seasonal variability of major emissions
128 sources and meteorology on predicted concentrations while keeping the resources required
129 for emissions inventory development at a feasible level.

Commented [ΠΣ3]: Referee #1 – Comment 2

Commented [BD4]: Referee #1 - Comment 1

130 We apply the Particulate Matter Comprehensive Air quality Model with Extensions
131 version 2.0 (PMCAMx-v2.0) to study the impact of increasing model resolution on the
132 ability to reproduce observed PM_{2.5} concentrations. We evaluate the PMCAMx predictions
133 at various grid resolutions against regulatory measurements of PM_{2.5} concentration and
134 composition, as well as measurements from a network of low-cost sensors (Zimmerman et
135 al., 2018) during February and July 2017 which provide a unique opportunity for
136 comparison not available to previous studies. Aerosol mass spectrometer (AMS)
137 measurements taken in Pittsburgh during February 2017 were also used to evaluate model
138 predictions.

139

140 2 Model Description

141 PMCAMx-v2.0, the Particulate Matter Comprehensive Air Quality Model with
142 Extensions (Karydis et al., 2010; Murphy and Pandis, 2010; Tsimpidi et al., 2010) is a
143 state-of-the-art atmospheric chemical transport model (CTM) that uses the framework of
144 the CAMx model (Environ, 2006) with advanced aerosol chemistry modules. [This model](#)
145 [uses detailed emissions and meteorology inputs to dynamically predict changes in pollutant](#)
146 [concentrations due to emissions, transport, chemical reactions in the gas and aqueous](#)
147 [phases, removal processes, and aerosol processes.](#) To track the dynamic evolution of
148 aerosol mass, 10 moving size sections are used (Gaydos et al., 2003). The chemical
149 mechanism SAPRC99 (Carter, 1999) was used for gas-phase chemistry, including 237
150 individual chemical reactions involving 91 chemical species. Aqueous-phase chemistry is
151 calculated with the Variable Size Resolution Model (Fahey and Pandis, 2001). PMCAMx-
152 v2.0 considers the formation of aerosol mass comprised of sulfate, nitrate, ammonium,
153 sodium, chloride, water, elemental carbon, as well as lumped organic species (both primary
154 and secondary). Inorganic aerosol growth is modelled using an approach that assumes
155 equilibrium between the bulk aerosol and gas phases. Partitioning of semivolatile inorganic
156 aerosol is calculated using ISORROPIA-I (Nenes et al., 1998). The Volatility Basis Set
157 (VBS) was used to calculate partitioning of organic aerosol components across a
158 distribution of species volatility (Donahue et al., 2006). Volatility bins (10) with effective
159 saturation concentration from 10⁻³ to 10⁶ μg m⁻³ (at 298 K) are used for primary organic
160 aerosol (POA). Secondary organic aerosol is split into anthropogenic (aSOA) and biogenic

Commented [BD5]: Referee #2 - Comment 2

161 (bSOA) components, formed from a variety of SOA-forming volatile organic compounds
162 (VOCs) from human activity and natural sources, respectively using NO_x-dependent SOA
163 formation yields (Lane et al., 2008). Both aSOA and bSOA are split into 4 volatility bins
164 with effective saturation concentration from 10⁰ to 10³ μg m⁻³ (at 298 K).

165

166 3 Model Application

167 Air quality simulations of a 5184 km² area comprised of southwestern Pennsylvania
168 and smaller parts of eastern Ohio and norther West Virginia were performed using
169 PMCAMx. Two distinct simulation periods of February and July 2017 were investigated.
170 The approach of Garcia et al. (2022) was used to produce speciated PM_{2.5} concentration
171 predictions at spatial resolution of 36 km, 12 km, 4 km, and 1 km. Surface-level boundary
172 conditions for the 36 x 36 km simulations are provided in Table S1. ~~Boundary conditions
173 for the higher resolution grids are taken from the results of parent grid simulations. The
174 first two days of simulation output have been removed from the analysis to allow for model
175 spin-up.~~

Commented [BD6]: Referee #1 - Comment 2

176 Meteorological fields were calculated using the Weather Research and Forecasting
177 model (WRF-v3.6.1) with horizontal resolution of 12 x 12 km, providing wind
178 components, eddy diffusivity, temperature, pressure, humidity, clouds, and precipitation
179 inputs for use in PMCAMx. Meteorology initial and boundary conditions were retrieved
180 from the ERA-Interim global climate re-analysis database. The United States Geological
181 Survey database was used to obtain input data for terrain, land-use, and soil type. When
182 necessary, WRF output was interpolated to higher resolutions. An evaluation of
183 interpolated meteorological inputs using data from METAR stations near the city of
184 Pittsburgh in southwestern Pennsylvania determined that errors in the magnitude and
185 phasing of diurnal cycles of temperature, relative humidity, and wind speed are
186 appropriately small for use in air quality studies. These results are provided in the
187 supplementary material (Fig. S1, S2).

Commented [ΠΣ7]: Referee # 2 – Comment 3

188 Anthropogenic emissions are derived from the 2017 projections of the 2011
189 National Emissions Inventory (Eyth and Vukovich, 2016) modelling platform. The Sparse
190 Matrix Operator Kernel Emissions modeling system (SMOKE) was used, along with
191 meteorological inputs to calculate emissions at a horizontal resolution of 12 x 12 km.

192 Default spatial surrogates were used to allocate these emissions to higher resolutions.
193 Custom surrogates were developed for commercial cooking and on-road traffic emissions
194 sectors within the 1 x 1 km grid and used for the primary analysis in this work. The use of
195 these new surrogates results in different spatial distribution of emissions for cooking and
196 on-road traffic sources than what would be observed with the default spatial surrogates.
197 Additional simulations were performed to quantify the impact of these proposed surrogates
198 on predicted PM_{2.5} concentrations.

Commented [BD8]: Referee #2 - Comment 4

Commented [BD9]: Referee #1 - Comment 2
Referee #2 - Comment 7

Commented [BD10]: Referee #2 - Comment 5

199 For commercial cooking, the normalized restaurant count was used to distribute the
200 emissions from the sector in space within the 1 x 1 km and 4 x 4 km domains. This surrogate
201 distributed commercial cooking emissions based on the density of restaurants identified by
202 the Google Places Application Programming Interface. To allocate on-road traffic
203 emissions, the output from the traffic model of Ma et al. (2020) was used. This model
204 simulates hourly traffic using data from the Pennsylvania Department of Transportation.
205 Emissions from the on-road traffic sector were then allocated based on these values.

Commented [BD11]: Referee #1 - Comment 4

206 207 **3.1 Available measurements for model evaluation**

208 Model predictions of sulfate, nitrate, elemental carbon and organic aerosol were
209 compared with measurements from 4 sites from the EPA Chemical Speciation Network
210 (EPA-CSN) (U.S. EPA, 2002). The locations of these 4 sites are shown in Figure 1a. These
211 sites include: Lawrenceville, an urban background site 4 km northeast of downtown
212 Pittsburgh; Hillman State Park located in a state park in southwest Pennsylvania in a rural
213 and remote location approximately 40 km upwind of Pittsburgh; Steubenville in the Ohio
214 River Valley close to industrial installations and coal-fired power plants, and the Liberty-
215 Clairton monitor, which is located close to the Clairton Coke Works in the Monongahela
216 River Valley 14 km southeast of downtown Pittsburgh. Speciated PM_{2.5} measurements
217 from EPA-CSN sites are available every three days during the simulation periods. Daily
218 non-speciated measurements of total PM_{2.5} mass concentration are available from 17 sites
219 within the inner simulation domain and are used to further evaluate total PM_{2.5} mass
220 concentration predictions. The locations of these sites are also shown in Figure 1a.

221 For February 2017, high-resolution AMS measurements from the Carnegie Mellon
222 University supersite (Gu et al., 2018) are used to evaluate the predicted chemical

223 composition of PM_{2.5} model predictions. Positive matrix factorization results are also used
224 to investigate the breakdown of organic aerosol components. AMS measurements were
225 taken continuously from February 1 to February 14, 2017. Due to uncertainties with the
226 AMS collection efficiency during this campaign, we use here only the fractional particle
227 composition data.

228 PMCAMx predictions of PM_{2.5} were also compared with measurements taken with
229 a network of Real-time Affordable Multi-Pollutant (RAMP) monitors (Zimmerman et al.,
230 2018) distributed in the city of Pittsburgh. During the winter period measurements at 7 sites
231 were available, all located within the boundaries of the city of Pittsburgh, while 22 sites
232 were in operation during the summer period with a few sites also outside the city (Fig. 1b).
233 Uncertainty in these low-cost measurements of PM_{2.5} mass concentration is between 3-4
234 $\mu\text{g m}^{-3}$ for hourly averaging times (Malings et al., 2019).

235 The model performance is assessed in terms of the mean bias (BIAS), the mean
236 error (ERROR), the fractional bias (FBIAS) and the fractional error (FERROR):

$$237 \quad \text{BIAS} = \frac{1}{N} \sum_{i=1}^N P_i - O_i \quad (1)$$

$$238 \quad \text{FBIAS} = \frac{2}{N} \sum_{i=1}^N \frac{P_i - O_i}{P_i + O_i} \quad (2)$$

$$239 \quad \text{ERROR} = \frac{1}{N} \sum_{i=1}^N |P_i - O_i| \quad (3)$$

$$241 \quad \text{FERROR} = \frac{2}{N} \sum_{i=1}^N \frac{|P_i - O_i|}{P_i + O_i} \quad (4)$$

240
242 where N is the number of valid measurements, P_i is the predicted concentration and O_i is
243 the corresponding observed concentration. The fractional error metric is bounded by 0
244 (perfect prediction performance) and 2.0 (extremely poor prediction performance).
245 Fractional bias is bounded by -2.0 (extreme underprediction) and +2.0 (extreme
246 overprediction).

247

248 **4 Evaluation of high-resolution model performance**

249 **4.1 Winter**

250 Table 1 summarizes the performance metrics of daily average PMCAMx-v2.0
251 PM_{2.5} predictions in the 1x1 km resolution, when compared with daily measurements from
252 EPA regulatory PM_{2.5} monitors. The speciated performance is illustrated in Figure 2.
253 Predictions of total PM_{2.5} mass perform well against regulatory measurements in the
254 February simulation period, with fractional error of 0.3 and fractional bias of +0.07.

255 Average measured PM_{2.5} sulfate for this time period was 1.9 µg m⁻³. Lower sulfate
256 levels were observed at the Lawrenceville site in Pittsburgh (1.2 µg m⁻³) while significantly
257 higher levels were observed at the Steubenville site (3.1 µg m⁻³). Predicted domain-average
258 PM_{2.5} sulfate at 1 x 1 km resolution was 1.3 µg m⁻³. Overall fractional error for sulfate
259 predictions was 0.41 and no overall bias was observed (fractional bias of -0.02). PM_{2.5}
260 sulfate was slightly overpredicted at Hillman State Park (+0.18 fractional bias) and
261 Lawrenceville (+0.25 fractional bias) and underpredicted at the industrial sites,
262 Steubenville (-0.24 fractional bias) and Liberty/Clairton (-0.43 fractional bias) where
263 observed PM_{2.5} sulfate concentrations were higher.

264 Overpredictions were seen for PM_{2.5} nitrate, with a fractional bias of +0.81. The
265 average measured concentration at EPA-CSN sites within the simulation domain was 1.5
266 µg m⁻³, while the domain-average predicted concentration was 1.8 µg m⁻³. Observed
267 average PM_{2.5} nitrate concentrations at Hillman State Park and Lawrenceville were slightly
268 lower at 1.1 µg m⁻³ and 1.2 µg m⁻³, respectively. Nitrate at the Steubenville location was
269 observed to be higher on average at 2.2 µg m⁻³. This overprediction is seen at all sites but
270 is particularly prevalent at Hillman State Park, Lawrenceville, and Liberty/Clairton, where
271 errors are of the order of a factor of two. Previous PMCAMx modeling studies have found
272 similar over-predictions. Part of this overprediction was due to the use of coarse-grid
273 resolution (Zakoura and Pandis, 2018), but this is unlikely to be the cause here, because
274 81% of the predicted domain-average nitrate is transported from outside of the inner
275 modeling domain. These inconsistencies in PM_{2.5} nitrate predictions are likely due to errors
276 in the partitioning of nitrate between the fine (PM_{2.5}) and coarse (PM₁₀) modes, resulting
277 in an overprediction of PM_{2.5} nitrate. Resolving this modeling error likely requires
278 improvements to the treatment of dust within the model, and the use of a dynamic approach
279 for inorganic aerosol calculations rather than the bulk equilibrium approach.

280 The behavior of PM_{2.5} ammonium measurements is similar to that of nitrate as most
281 of it is in the form of ammonium nitrate. The average measured concentration at the four
282 EPA-CSN stations was 0.9 μg m⁻³. At Hillman State Park and Lawrenceville, the measured
283 average was lower at 0.5 μg m⁻³ but higher at the Liberty/Clairton location at 2.1 μg m⁻³.
284 PM_{2.5} ammonium was overpredicted similarly to PM_{2.5} nitrate with +0.83 fractional bias.
285 The average measured concentration of PM_{2.5} elemental carbon at EPA-CSN sites during
286 February 2017 was 1.1 μg m⁻³. Elemental carbon concentrations are more localized than
287 the inorganic PM_{2.5} components. At Hillman State Park the average measured
288 concentration was only 0.5 μg m⁻³ while at Liberty/Clairton the averaged measured
289 concentration was 2.9 μg m⁻³. For elemental carbon, the predicted domain-average was 0.4
290 μg m⁻³. Average elemental carbon concentration in the 4 x 4 km simulation grid outside of
291 the inner modeling domain was 0.3 μg m⁻³. Black carbon predictions at all sites had a
292 fractional error of 0.71 with fractional bias of -0.08. Elemental carbon was overpredicted
293 at the urban site with fractional bias of 0.73 and underpredicted at the other sites.

294 Average measured OA during this period was 4.4 μg m⁻³, but with significant
295 spatial variability. At Hillman State Park and Lawrenceville measured OA was 3.1 μg m⁻³
296 and 3.4 μg m⁻³, respectively. At Liberty/Clairton and Steubenville the average measured
297 OA was 7 μg m⁻³ and 6.3 μg m⁻³, respectively. Domain-average predicted OA was 2.2 μg
298 m⁻³. Outside of the inner 1 x 1 km domain, average predicted OA was 1.6 μg m⁻³,
299 suggesting that the majority of predicted OA is transported from outside of the 1 x 1 km
300 grid. Overall OA prediction performance in the winter is acceptable at 0.53 fractional error
301 and low fractional bias (-0.01). At individual sites, performance varies. OA is predicted
302 with low fractional bias (-0.10) at the rural Hillman State Park site. OA is overpredicted by
303 with +0.31 fractional bias at the urban site in Lawrenceville and underpredicted at both
304 industrial sites. An added degree of uncertainty exists with the industrial sites within the
305 inner domain. The emissions from these sources may be underestimated in the inventory
306 and these locations are also difficult to accurately model due to their geographic location
307 in river valleys.

308 Average concentrations of PM_{2.5} sulfate, nitrate, and ammonium in the 4 x 4 km
309 resolution domain were around 83% of the average predicted concentrations in the inner 1
310 x 1 km simulation grid. For elemental carbon and OA, the outer concentration was 64%

311 and 73% of the inner concentration respectively, indicating that these species had
312 significant local sources. For these more local pollutants, the model appears to perform
313 well in terms of capturing urban-rural gradients, but with a tendency towards
314 underprediction at the rural site in Hillman State Park and overprediction at the urban site
315 in Lawrenceville. The model also underpredicts EC and OA at the industrial locations,
316 especially elemental carbon (-0.67 and -1.02 fractional bias at Steubenville and
317 Liberty/Clairton, respectively). This again suggests errors in the emissions inventory or
318 problems in simulating atmospheric dispersion near the sources.

319 Comparisons with the PM₁ composition as determined by the AMS from February
320 3 through February 14, 2017, show excellent agreement for all species (Fig. 3a). Gu et al.
321 (2018) used PMF analysis and allocated total measured OA into five factors. Three of them
322 corresponded to primary organic aerosol: hydrocarbon-like OA (HOA), cooking OA
323 (COA) and biomass burning OA (BBOA) and two secondary OA factors: more-oxidized
324 organic aerosol (MO-OOA) and less-oxidized organic aerosol (LO-OOA). To compare
325 PMCAMx predictions with the primary PMF factors, two additional simulations were
326 performed in which emissions from biomass burning and commercial cooking were set to
327 zero. The predicted concentrations were then subtracted from the base case to estimate the
328 contribution from each respective source. The remaining primary OA was assigned to
329 HOA. The LO-OOA and MO-OOA factors were added together and compared with the
330 PMCAMx SOA predictions.

331 The predicted cooking OA (COA) at the CMU site is 25% of the total OA and is in
332 agreement with the PMF/AMS estimate of 22% (Fig. 3b). This is encouraging given the
333 small bias of the model for total OA levels. The predicted HOA and BBOA are higher than
334 measured by a factor of 2 or more. At the same time, the measurements indicate a
335 surprisingly high contribution of SOA (53% of the total OA) during a period with little
336 photochemical activity and low levels of OH radicals. SOA is predicted to be just 20% of
337 the total during this time period. These discrepancies may indicate transformation of the
338 HOA and BBOA to OOA during this wintertime period, that are not included in the model.

339 Kodros et al. (2020+) recently suggested that BBOA can react with the NO₃ radical during
340 the winter and can be transformed to OOA.

341

342 **4.2 Summer**

343 Total PM_{2.5} mass concentrations are underpredicted in the summer period. The
344 average measured PM_{2.5} value in the regulatory network in the area was 11.4 µg m⁻³, while
345 the average predicted value at the regulatory sites was 4 µg m⁻³ lower.

346 Speciated PM_{2.5} performance is illustrated in Figure 4. Average measured PM_{2.5}
347 sulfate for the summer period was 2 µg m⁻³. Slightly lower levels were observed at the
348 Lawrenceville site in Pittsburgh (1.9 µg m⁻³). Liberty/Clairton had higher measured sulfate
349 concentrations (2.6 µg m⁻³), but this difference between locations is lower than what was
350 observed in the winter period. Predicted domain-average PM_{2.5} sulfate at 1 x 1 km
351 resolution was 1.3 µg m⁻³. Overall fractional error (0.62) and fractional bias (-0.21) for
352 sulfate predictions was higher than in the winter simulation period. PM_{2.5} sulfate was
353 underpredicted at all sites but to the largest extent at Hillman State Park (-0.36 fractional
354 error).

355 Overpredictions of PM_{2.5} nitrate were also seen the summer period, and at all types
356 of sites. Average measured PM_{2.5} nitrate was 0.3 µg m⁻³, much lower than in the winter.
357 The domain-average predicted PM_{2.5} nitrate was 0.7 µg m⁻³. Again, predicted PM_{2.5} nitrate
358 in the inner domain is dominated by material transported from outside the boundaries
359 (75%), so the issue is not resolved by using a high-resolution grid. Improvements to PM_{2.5}
360 nitrate formation are needed in the form of dust models with increased complexity to
361 resolve the issues with fine-coarse mode partitioning of particulate nitrate. These issues
362 have been highlighted by decreased concentrations of PM_{2.5} pollution in recent years.

363 Observed PM_{2.5} ammonium concentrations at EPA-CSN sites were also much
364 lower in the summer with an average value of 0.5 µg m⁻³. Slightly higher average
365 concentrations were observed at Liberty/Clairton (0.7 µg m⁻³) and slightly lower
366 concentrations were observed at Steubenville (0.4 µg m⁻³). The domain-average predicted
367 PM_{2.5} ammonium concentration was 0.6 µg m⁻³. The average concentration directly outside
368 of the inner domain was 0.5 µg m⁻³. Overall performance was better for ammonium in the
369 summer than in the winter with fractional error of 0.62 and fractional bias of +0.44. The
370 strongest overprediction is seen at the Steubenville site (+0.57 fractional bias).

371 The average measured elemental carbon (EC) concentration in July was 0.7 µg m⁻³
372 ³. Measured EC carbon was significantly higher at Liberty/Clairton (1 µg m⁻³) and lower

373 at rural Hillman State Park ($0.4 \mu\text{g m}^{-3}$). Domain-average predicted EC was $0.3 \mu\text{g m}^{-3}$.
374 Outside of the inner domain, the average predicted concentration was $0.2 \mu\text{g m}^{-3}$. Elemental
375 carbon predictions in July had a lower fractional error compared to the winter at 0.60 but
376 showed a stronger negative fractional bias at -0.33. The model severely underpredicts at
377 Hillman State Park (-0.86 fractional bias), where measured concentrations were lowest, but
378 also at the industrial sites of Steubenville (-0.55 fractional bias) and Liberty/Clairton (-0.65
379 fractional bias). EC was slightly overpredicted at the urban Lawrenceville location (+0.14
380 fractional bias). While the urban-rural gradient in EC is slightly overpredicted, the model
381 is still able to capture well the variability between rural (Hillman State Park) and urban
382 (Lawrenceville). The model struggles to reproduce high measurements of EC at the
383 Steubenville site, reiterating the issues with industrial EC seen in the winter.

384 Average measured OA concentration was $4.5 \mu\text{g m}^{-3}$ in July. Higher concentrations
385 were observed at the industrial sites, Liberty/Clairton and Steubenville ($5.0 \mu\text{g m}^{-3}$)
386 respectively. The lowest observed concentration was in Hillman State Park ($3.6 \mu\text{g m}^{-3}$).
387 The average predicted concentration at CSN sites was $2.7 \mu\text{g m}^{-3}$. On average, OA is
388 underpredicted with fractional bias of -0.47. This underprediction occurs at all sites but is
389 less prevalent at the urban Lawrenceville location (-0.19 fractional bias) and is most
390 dramatic in Steubenville (-0.65 fractional bias). Because such a large fraction of the OA in
391 the summer is predicted to be secondary (50% of local OA on average) and transported
392 from outside of the inner modeling domain (84% of total OA), treatment of SOA formation
393 is likely a key factor contributing to the underprediction of $\text{PM}_{2.5}$ in the summer. While
394 these improvements are necessary for overall model improvement, they do not have
395 significant impact on the urban-rural gradients which are the focus of this work and are
396 driven by primary species. The performance of EC predictions in various locations is
397 encouraging with regards to primary $\text{PM}_{2.5}$ performance.

398

399 **5 Effect of grid resolution on $\text{PM}_{2.5}$ performance**

400 To determine the effect of grid resolution on the ability of the model to resolve
401 geographical variations in $\text{PM}_{2.5}$ concentrations, daily average measurements from the 17
402 EPA regulatory sites were compared with PMCAMx predictions from simulations at 36

403 km, 12 km, 4 km and 1 km. The PMCAMx performance metrics are summarized in Table
404 2.

405

406 **5.1 Winter**

407 During the winter period, increasing grid resolution reduces the average fractional
408 error from 34% at 36 x 36 km to 30% at 1 x 1 km. The higher resolution also improved the
409 fractional bias, from -0.09 at 36 x 36 km to +0.05 at 1 x 1 km. The performance is illustrated
410 in Figure 5. Performance at urban locations stayed steady in the winter, with fractional
411 error changing from 0.30 to 0.26 and fractional bias changing from +0.02 to +0.08 moving
412 from 36 km to 1 km resolution (Fig. S3). Rural performance improved to a greater extent,
413 with fractional error improving from 0.33 to 0.28 and fractional bias lowering from +0.21
414 to +0.11.

415 The comparison with low-cost sensor measurements largely represents the
416 performance of the model in terms of urban PM_{2.5} predictions. The performance metrics of
417 PMCAMx-v2.0 when compared to measurements from low-cost sensors are shown in
418 Table 3. Moving from low to high resolution, the predictions go from no bias (-0.02) to a
419 bias of +0.24. Due to the slight overprediction of the urban-rural gradient seen earlier
420 (particularly with EC), the high resolution would likely lead to more positive biases when
421 compared to a largely urban network. Fractional error increases slightly, but still exhibits
422 good performance moving from 0.33 to 0.37.

423

424 **5.2 Summer**

425 In the summer period, (Fig. 6) the model performance improved as the resolution
426 increased from 36 km to 1 km. Fractional error decreased from 0.53 to 0.48, while
427 fractional bias increased from -0.46 to -0.39. In July, performance at the urban locations
428 significantly increased with resolution (Fig. S4). Fractional error decreased from 52% at
429 36 x 36 km to 0.42 at 1 x 1 km. Fractional bias also improved from -0.46 at the coarse grid
430 resolution to -0.39 at the finest scale. Rural predictions of PM_{2.5} were also better with
431 increasing resolution in the summer. Fractional error decreased from 0.31 to 0.22 while
432 fractional bias decreased from +0.05 to -0.05.

433 Larger improvements are seen with increasing resolution during the summer when
434 compared to measurements from low-cost sensors. Starting from a large negative bias of
435 $-5.4 \mu\text{g m}^{-3}$ (fractional bias of -0.48) at the 36 x 36 km resolution, performance consistently
436 improved with each increasing resolution step with the bias eventually reaching $-3.7 \mu\text{g}$
437 m^{-3} (fractional bias of -0.27) at the 1 x 1 km. There was also a reduction in fractional error
438 from 0.52 at the coarse to 0.41 at the fine 1 x 1 km resolution. These metrics are
439 encouraging, although they are likely impacted by an overprediction of the urban-rural
440 gradient, similar to winter. Improvement of the secondary $\text{PM}_{2.5}$ predictions is still the
441 largest source of error between predictions and this source of measurements.

442

443 **6 Evaluation of Novel Emissions Surrogates**

444 For commercial cooking, the normalized restaurant count was used to distribute the
445 emissions from the sector in space within the 1 x 1 km domain. Geographical information
446 was collected for all restaurant locations in the inner domain from the Google Places
447 Application Programming Interface. This includes southwestern Pennsylvania as well as
448 parts of eastern Ohio and northern West Virginia. To allocate on-road traffic emissions, the
449 output from the traffic model of Ma et al. (2020) was used. This model simulated hourly
450 traffic using data from the Pennsylvania Department of Transportation sites located
451 throughout the inner modeling domain. ~~Changes in the spatial distribution of cooking and~~
452 ~~on-road traffic emissions are illustrated in the supplementary material (Fig. S5-S8). The~~
453 ~~use of new surrogates resulted in a new spatial distribution of emissions for both cooking~~
454 ~~and on-road traffic sources when compared to those developed using default~~
455 ~~emissions surrogates. The changes in spatial distributions are illustrated in the~~
456 ~~supplementary material (Figures S5, S6, S7, and S8).~~ These novel emissions surrogates
457 resulted in larger emissions of both traffic and cooking in the downtown area. In the case
458 of on-road traffic, major highways in the inner domain are emphasized with the new
459 surrogates.

460 For both February and July 2017, the largest observed change when using the novel
461 surrogates is an increase in predicted $\text{PM}_{2.5}$ of around $3 \mu\text{g m}^{-3}$ in the downtown Pittsburgh
462 area (Fig. 7). Differences in predicted $\text{PM}_{2.5}$ concentrations outside of the urban areas of
463 the inner domain are very small (less than $0.5 \mu\text{g m}^{-3}$ in magnitude).

Commented [BD12]: Referee #2 - Comment 1
Referee #2 - Comment 4

464 Model performance at 1 x 1 km resolution is detailed in Table 4. Negligible changes
465 in performance were seen using EPA regulatory PM_{2.5} data in February 2017. Small
466 improvements were seen at regulatory sites in July 2017, where fractional error was
467 reduced from 51% to 48% and fractional bias increased from -43% to -39%. A positive
468 shift in fractional bias was seen with the use of the new surrogates during both periods
469 when compared to low-cost sensor measurements, resulting in a modest overprediction of
470 PM_{2.5} in the winter (+0.24 fractional bias) and a modest underprediction of PM_{2.5} in the
471 summer (-0.27 fractional bias). The larger changes when compared to the low-cost sensor
472 measurements are a result of the location of the low-cost sensors in urban areas, where the
473 new surrogates predicted elevated PM_{2.5} mass concentrations.

474 7 Conclusions

475 We applied PMCAMx-v2.0 over southwestern Pennsylvania during February and
476 July 2017 at grid resolutions of 36 km, 12 km, 4 km and 1 km. Emissions were calculated
477 for the relevant grids by using the spatial surrogates provided along with the 2011 NEI for
478 all emissions sectors except traffic and cooking, for which 1 x 1 km spatial surrogates were
479 developed.

480 PMCAMx predicts winter sulfate, elemental carbon, and organic aerosol
481 concentrations with fractional biases below 10% at high resolution. Nitrate concentrations
482 are overpredicted (bias +1.4 $\mu\text{g m}^{-3}$) following the trend of previous studies in both the US
483 and Europe. Agreement with total PM_{2.5} measurements is also encouraging with a
484 fractional bias of +5%. Variability between urban and rural predictions of local pollutants
485 EC and organic aerosol (OA) are reproduced well in the winter period. Underpredictions
486 of summer OA concentrations led to underpredictions of total PM_{2.5} mass. Summer sulfate
487 is reproduced with fractional bias of -21% and elemental carbon (EC) is predicted with
488 fractional bias of -33%. Nitrate is similarly overpredicted in the summer with fractional
489 bias of +70% although with a much smaller magnitude than in the winter (+0.4 $\mu\text{g m}^{-3}$).
490 ~~Improvement of the treatment of dust in the model is required to better model the~~
491 ~~distribution of particulate nitrate between PM_{2.5} and PM₁₀ modes.~~ Differences between
492 urban and rural EC is also predicted well in the summer, while OA is predicted to vary
493 little between urban and rural locations. This is indicative of a greater contribution of
494 secondary species to OA during this period. ~~Improvements to SOA formation chemistry~~

495 ~~within the model, particularly from biogenic sources outside of the inner modeling domain,~~
496 ~~will likely have a significant impact on PM_{2.5} predictions around the city of Pittsburgh.~~
497 ~~This, along with the improvement of dust treatment in the model, are topics of future work~~
498 ~~for model improvement.~~
499

500 PM_{2.5} prediction performance improved in almost all cases when increasing
501 the resolution from 36 km to 1 km. Underpredictions at urban sites and overpredictions at
502 rural sites were reduced at the same time. This is true when comparing against
503 measurements from regulatory sites as well as low-cost monitors. The improved
504 performance here is evidence of the enhanced ability of the model to capture important
505 urban-rural gradients in PM_{2.5} pollution by increasing the resolution of predictions to 1 x 1
506 km. Increasing resolution of predictions has been shown here to improve model
507 performance when comparing predicted PM_{2.5} concentrations with observations from
508 regulatory monitors and low-cost sensors. However, these simulations highlight the need
509 for specific additional improvements in the simulation to some of the secondary PM_{2.5}
510 formation pathways in the model. Improvement of the treatment of dust in the model is
511 required to better simulate the distribution of particulate nitrate between the fine and
512 coarse PM_{2.5} and PM₁₀ modes. Additionally, improvements to SOA formation chemistry
513 within the model, particularly from biogenic sources outside of the inner modeling domain,
514 will likely have a significant impact on PM_{2.5} predictions in around the city of Pittsburgh.

515

516

517 *Code Availability.* The PMCAMx-v2.0 code is available in Zenodo at
518 <https://doi.org/10.5281/zenodo.6772851> (Dinkelacker et al., 2022). License (for files):
519 GNU General Public License v3.0.

520

521 *Author contributions.* BTD performed the PMCAMx simulations, analyzed the results, and
522 wrote the manuscript. PGR wrote the code for data analysis, prepared anthropogenic
523 emissions and other inputs for the PMCAMx simulations, and assisted in writing the
524 manuscript. IK set up the WRF simulations and assisted in the preparation of the

Commented [BD13]: Referee #1 - Comment 3

525 meteorological inputs. SNP and PJA designed and coordinated the study and helped in the
526 writing of the paper. All authors reviewed and commented on the manuscript.

527

528 *Competing Interests.* The authors declare that they have no conflict of interest.

529 *Financial support.* This work was supported by the Center for Air, Climate, and Energy
530 Solutions (CACES) which was supported under Assistance Agreement No. R835873
531 awarded by the U.S. Environmental Protection Agency and the Horizon-2020 Project
532 REMEDIA of the European Union under grant agreement No 874753.

533

534 **References**

535 Allan, J. D.; Williams, P. I.; Morgan, W. T.; Martin, C. L.; Flynn, M. J.; Lee, J.; Nemitz,
536 E.; Phillips, G. J.; Gallagher, M. W.; Coe, H.: Contributions from transport, solid
537 fuel burning and cooking to primary organic aerosols in two UK cities, *Atmos.*
538 *Chem. Phys.*, 10, 647-668. doi:10.5194/acp-10-647-2010, 2010.

539 Anand, S.: The concern for equity in health, *JECH*, 56, 485–487.
540 doi:10.1136/jech.56.7.485, 2002.

541 Arunachalam, S., Holland, A., Do, B., Abraczinskas, M.: A quantitative assessment of the
542 influence of grid resolution on predictions of future-year air quality in North
543 Carolina, USA, *Atmos. Environ.*, 40, 5010–5026.
544 doi:10.1016/j.atmosenv.2006.01.024, 2006.

545 Carter, W.P.L.: Documentation of the SAPRC-99 chemical mechanism for VOC reactivity
546 assessment., 1999.

547 [Day, M.C., Pandis, S.N.: Effects of a changing climate on summertime fine particulate
548 matter levels in the eastern U.S., *J. Geophys. Res.*, 120, 5706–5720.
549 doi:10.1002/2014JD022889, 2015.](#)

550 Dinkelacker, B.T., Garcia Rivera, P., Kioutsioukis, I., Adams, P., Pandis, S.N.: Source
551 Code for PMCAMx-v2.0: "High-resolution modeling of fine particulate matter in
552 an urban area using PMCAMx-v2.0", Zenodo [model code],
553 <https://doi.org/10.5281/zenodo.6772851>, 2022.

554 Dockery, D.W., Pope, C.A.: Acute Respiratory Effects of Particulate Air Pollution, *Annu.*
555 *Rev. Public Health*, 15, 107–132. doi:10.1146/annurev.pu.15.050194.000543,

Commented [ΠΣ14]: Referee #1 – Comment 7

556 1994.

557 Donahue, N.M., Robinson, A.L., Stanier, C.O., Pandis, S.N.: Coupled partitioning,
558 dilution, and chemical aging of semivolatile organics, *Environ. Sci. Technol.*, 40,
559 2635–2643. doi:10.1021/es052297c, 2006.

560 ENVIRON: CAMx (Comprehensive Air Quality Model with Extensions) User's Guide
561 Version 4.20, 2006.

562 Eyth, A., Vukovich, J.: Technical Support Document (TSD): Preparation of emissions
563 inventories for the version 6.2, 2011 emissions modeling platform., 2016.

564 Fahey, K. M.; Pandis, S. N.: Optimizing model performance: variable size resolution in
565 cloud chemistry modeling, *Atmos. Environ.*, 35, 4471-4478, doi:10.1016/S1352-
566 2310(01)00224-2, 2001.

567 Fountoukis, C., Koraj, D., Denier van der Gon, H.A.C., Charalampidis, P.E., Pilinis, C.,
568 Pandis, S.N.: Impact of grid resolution on the predicted fine PM by a regional 3-D
569 chemical transport model, *Atmos. Environ.*, 68, 24–32.
570 doi:10.1016/j.atmosenv.2012.11.008, 2013.

571 Garcia Rivera, P., Dinkelacker, B. T., Kioutsioukis, I., Adams, P. J., and Pandis, S. N.:
572 Source-resolved variability of fine particulate matter and human exposure in an
573 urban area, *Atmos. Chem. Phys.*, 22, doi:10.5194/acp-22-2011-2022, 2022.

574 Gaydos, T.M.; Koo, B.; Pandis, S.N.; Chock, D.P.: Development and applicaiton of an
575 efficient moving sectional approach for the solution of the atmospheric aerosol
576 condensation/evaporation equations, *Atmos. Environ.*, 37, 3303-3316,
577 doi:10.1016/S1352-2310(03)00267-X, 2003.

578 Gu, P., Li, H.Z., Ye, Q., Robinson, E.S., Apte, J.S., Robinson, A.L., Presto, A.A.: Intracity
579 variability of particulate matter exposure is driven by carbonaceous sources and
580 correlated with land-use variables, *Environ. Sci. Technol.*, 52, 11545–11554.
581 doi:10.1021/acs.est.8b03833, 2018.

582 Karydis, V.A., Tsimpidi, A.P., Fountoukis, C., Nenes, A., Zavala, M., Lei, W., Molina,
583 L.T., Pandis, S.N.: Simulating the fine and coarse inorganic particulate matter
584 concentrations in a polluted megacity, *Atmos. Environ.*, 44, 608–620.
585 doi:10.1016/j.atmosenv.2009.11.023, 2010.

586 [Kodros, J.K., Papanastasiou, D.K., Paglione, M., Masiol, M., Squizzato, S., Florou, K.,](#)

587 [Skyllakou, K., Kaltsonoudis, C., Nenes, A., Pandis, S.N.: Rapid dark aging of](#)
588 [biomass burning as an overlooked source of oxidized organic aerosol, Proc. Natl.](#)
589 [Acad. Sci., 117\(52\), 33028-33033, doi:10.1073/pnas.2010365117, 2020.](#)

590 Kumar, N., Russell, A.G.: Multiscale air quality modeling of the Northeastern United
591 States, *Atmos. Environ.*, 30, 1099–1116. doi:10.1016/1352-2310(95)00317-7,
592 1996.

593 Lane, T.E., Donahue, N.M., Pandis, S.N.: Effect of NO_x on secondary organic aerosol
594 concentrations, *Environ. Sci. Technol.*, 42, 6022–6027. doi:10.1021/es703225a,
595 2008.

596 Lanz, V. A.; Alfarra, M. R.; Baltensperger, U.; Buchmann, B.; Hueglin, C.; Prevot, A. S.
597 H.: Source apportionment of submicron organic aerosols at an urban site by factor
598 analytical modelling of aerosol mass spectra, *Atmos. Chem. Phys.*, 7, 1503-1522.
599 doi:10.5194/acp-7-1503-2007, 2007.

600 Ma, W., Pi, X., Qian, S.: Estimating multi-class dynamic origin-destination demand
601 through a forward-backward algorithm on computational graphs. *Transportation*
602 *Research Part C: Emerging Technologies*, 119, 102747, doi:10.1016/j.trc.2020.
603 102747, 2020.

604 Malings, C., Tanzer, R., Haurlyliuk, A., Saha, P.K., Robinson, A.L., Presto, A.A.,
605 Subramanian, R.: Fine particle mass monitoring with low-cost sensors: corrections
606 and long-term performance evaluation, *Aerosol Sci. Tech.*, 54, 160-174, doi:
607 10.1080/02786826.2019.1623863, 2019.

608 Murphy, B.N., Pandis, S.N.: Exploring summertime organic aerosol formation in the
609 eastern United States using a regional-scale budget approach and ambient
610 measurements, *J. Geophys. Res.*, 115, D24 doi:10.1029/2010JD014418, 2010.

611 Nenes, A., Pandis, S.N., Pilinis, C.: ISORROPIA: a new thermodynamic equilibrium
612 model for multiphase multicomponent inorganic aerosols, *Aquat. Geochem.*, 4,
613 123–152, doi:10.1023/A:1009604003981, 1998.

614 Pan, S., Choi, Y., Roy, A., Jeon, W.: Allocating emissions to 4 km and 1 km horizontal
615 spatial resolutions and its impact on simulated NO_x and O₃ in Houston, TX. *Atmos.*
616 *Environ.*, 164, 398–415, 2017.

617 Robinson, E.S., Gu, P., Ye, Q., Li, H.Z., Shah, R.U., Apte, J.S., Robinson, A.L., Presto,

Commented [BD15]: Referee #1 - Comment 6

- 618 A.A.: Restaurant Impacts on Outdoor Air Quality: Elevated Organic Aerosol Mass
619 from Restaurant Cooking with Neighborhood-Scale Plume Extents, *Environ. Sci.*
620 *Technol.*, 52, 9285–9294, doi:10.1021/acs.est.8b02654, 2018.
- 621 ~~Skylakou, K., Garcia Rivera, P., Dinkelacker, B., Karnezis, E., Kioutsioukis, I., Hernandez,~~
622 ~~C., Adams, P. J., Pandis, S. N.: Changes in PM_{2.5} concentrations and their sources~~
623 ~~in the US from 1990 to 2010, *Atmos. Chem. Phys.*, 21, 17115–17132,~~
624 ~~doi:10.5194/acp-21-17115-2021, 2021.~~
- 625 Stroud, C.A., Makar, P.A., Moran, M.D., Gong, W., Gong, S., Zhang, J., Hayden, K.,
626 Mihele, C., Brook, J.R., Abbatt, J.P.D., Slowik, J.G.: Impact of model grid spacing
627 on regional- and urban- scale air quality predictions of organic aerosol, *Atmos.*
628 *Chem. Phys.*, 11, 3107–3118, doi:10.5194/acp-11-3107-2011, 2011.
- 629 Tsimpidi, A.P., Karydis, V.A., Zavala, M., Lei, W., Molina, L.T., Ulbrich, I.M., Jimenez,
630 J.L., Pandis, S.N.: Evaluation of the volatility basis-set approach for the simulation
631 of organic aerosol formation in the Mexico City metropolitan area, *Atmos. Chem.*
632 *Phys. Disc.*, 9, 13693–13737, doi:10.5194/acpd-9-13693-2009, 2010.
- 633 U.S. EPA: User guide: Air Quality System, Report, Research Triangle Park, N.C., available
634 at: <http://www.epa.gov/ttn/airs/airsaqs/manuals/AQSUserGuide.pdf> (last access:
635 January 2022), 2002.
- 636 Zakoura, M., Pandis, S.N.: Improving fine aerosol nitrate predictions using a Plume-in-
637 Grid modeling approach, *Atmos. Environ.*, 215, 116887. doi:10.1016/
638 j.atmosenv.2019.116887, 2019.
- 639 Zakoura, M., Pandis, S.N.: Overprediction of aerosol nitrate by chemical transport models:
640 The role of grid resolution, *Atmos. Environ.*, 187, 390–400, doi:10.1016/
641 j.atmosenv.2018.05.066, 2018.
- 642 Zimmerman, N., Presto, A.A., Kumar, S.P.N., Gu, J., Hauryliuk, A., Robinson, E.S.,
643 Robinson, A.L., Subramanian, R.: A machine learning calibration model using
644 random forests to improve sensor performance for lower-cost air quality
645 monitoring, *Atmos. Meas. Tech.*, 11, 291–313, doi:10.5194/amt-11-291-2018,
646 2018.
- 647
648

649 **Table 1.** Comparison of daily average high-resolution PMCAMx-v2.0 predictions with
 650 daily EPA-CSN measurements during February and July 2017.
 651

February 2017						
	Sulfate	Nitrate	Ammon.	Elemental Carbon	Organic Aerosol	PM_{2.5}^a
Measured Avg. ($\mu\text{g m}^{-3}$)	1.92	1.51	0.91	1.08	4.37	10.34
Predicted Avg. ($\mu\text{g m}^{-3}$)	1.70	2.90	1.62	0.94	3.68	10.52
Error ($\mu\text{g m}^{-3}$)	0.79	1.54	1.03	0.78	2.15	3.02
Fractional Error	0.41	0.83	0.96	0.71	0.53	0.30
Bias ($\mu\text{g m}^{-3}$)	-0.22	1.40	0.71	-0.14	-0.68	0.18
Fractional Bias	-0.02	0.81	0.83	-0.08	-0.01	0.05

July 2017						
	Sulfate	Nitrate	Ammon.	Elemental Carbon	Organic Aerosol	PM_{2.5}^a
Measured Avg. ($\mu\text{g m}^{-3}$)	2.04	0.26	0.53	0.74	4.46	11.24
Predicted Avg. ($\mu\text{g m}^{-3}$)	1.60	0.68	0.79	0.56	2.67	7.26
Error ($\mu\text{g m}^{-3}$)	1.12	0.45	0.39	0.39	2.46	4.67
Fractional Error	0.62	0.82	0.62	0.60	0.67	0.49
Bias ($\mu\text{g m}^{-3}$)	-0.44	0.42	0.26	-0.18	-1.85	-4.01
Fractional Bias	-0.21	0.70	0.44	-0.33	-0.47	-0.39

653 ^a Measurements from the regulatory EPA monitors.
 654

655 **Table 2.** Comparison of daily average PMCAMx-v2.0 predicted PM_{2.5} concentrations
 656 during February and July 2017 with daily measurements from 17 EPA regulatory
 657 monitors.
 658

	36 x 36 km	12 x 12 km	4 x 4 km	1 x 1 km
February 2017				
Measured Avg. ($\mu\text{g m}^{-3}$)	10.34	10.34	10.34	10.34
Predicted Avg. ($\mu\text{g m}^{-3}$)	9.78	9.68	10.49	10.52
Error ($\mu\text{g m}^{-3}$)	3.35	3.16	3.04	3.02
Fractional Error	0.34	0.32	0.30	0.30
Bias ($\mu\text{g m}^{-3}$)	-0.56	-0.66	0.15	0.18
Fractional Bias	-0.09	-0.10	0.06	0.05
July 2017				
Measured Avg. ($\mu\text{g m}^{-3}$)	11.24	11.24	11.24	11.24
Predicted Avg. ($\mu\text{g m}^{-3}$)	6.90	6.86	7.26	7.23
Error ($\mu\text{g m}^{-3}$)	4.89	5.05	4.67	4.65
Fractional Error	0.53	0.53	0.49	0.48
Bias ($\mu\text{g m}^{-3}$)	-4.34	-4.39	-3.98	-4.01
Fractional Bias	-0.45	-0.47	-0.39	-0.39

659

660 **Table 3.** Comparison of daily average PMCAMx-v2.0 predicted PM_{2.5} concentrations
 661 during February and July 2017 with daily low-cost sensor (RAMP) measurements.
 662

	36 x 36 km	12 x 12 km	4 x 4 km	1 x 1 km
February 2017				
Measured Avg. ($\mu\text{g m}^{-3}$)	11.65	11.65	11.65	11.65
Predicted Avg. ($\mu\text{g m}^{-3}$)	10.23	11.64	12.04	13.50
Error ($\mu\text{g m}^{-3}$)	4.53	4.53	4.51	5.12
Fractional Error	0.33	0.33	0.34	0.37
Bias ($\mu\text{g m}^{-3}$)	-1.43	-0.02	0.4	1.85
Fractional Bias	-0.02	<0.01	0.14	0.24
July 2017				
Measured Avg. ($\mu\text{g m}^{-3}$)	12.59	12.59	12.59	12.59
Predicted Avg. ($\mu\text{g m}^{-3}$)	7.19	7.44	8.06	8.83
Error ($\mu\text{g m}^{-3}$)	5.60	5.70	5.29	4.89
Fractional Error	0.51	0.51	0.46	0.42
Bias ($\mu\text{g m}^{-3}$)	-5.40	-5.15	-4.53	-3.76
Fractional Bias	-0.48	-0.43	-0.36	-0.27

663
 664

665 **Table 4.** Performance of daily average predicted total PM_{2.5} concentrations compared to
 666 daily measurements from regulatory sites and low-cost sensors with the use of old
 667 surrogates and new surrogates for on-road traffic and commercial cooking [within the 1 x](#)
 668 [1 km resolution grid.](#)
 669

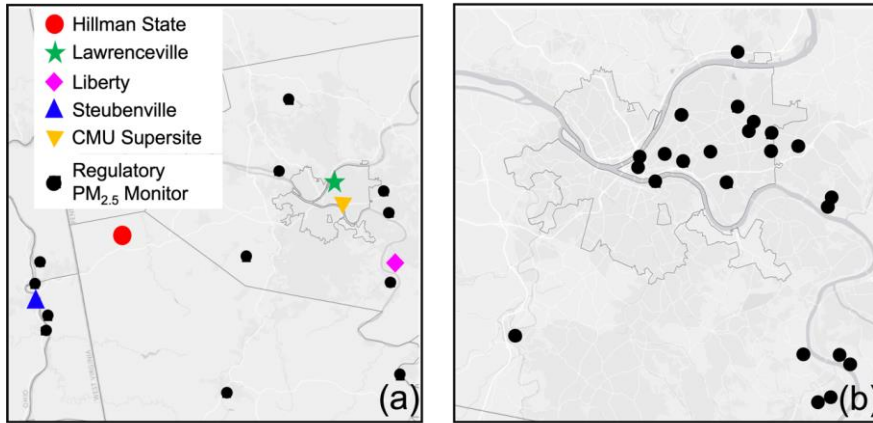
Commented [BD17]: Referee #2 - Comment 8

February 2017				
	Old Surrogates		New Surrogates	
	Regulatory network	Low-cost sensors	Regulatory network	Low-cost sensors
Observed Average ($\mu\text{g m}^{-3}$)	10.34	11.65	10.34	11.65
Predicted Average ($\mu\text{g m}^{-3}$)	10.23	11.32	10.52	13.50
Error ($\mu\text{g m}^{-3}$)	2.94	4.12	3.02	5.12
Fractional Error	0.29	0.31	0.30	0.37
Bias ($\mu\text{g m}^{-3}$)	-0.11	-0.33	0.18	1.85
Fractional Bias	-0.04	0.08	0.05	0.24

July 2017				
	Old Surrogates		New Surrogates	
	Regulatory network	Low-cost sensors	Regulatory network	Low-cost sensors
Observed Average ($\mu\text{g m}^{-3}$)	11.24	12.58	11.24	12.58
Predicted Average ($\mu\text{g m}^{-3}$)	7.09	7.98	7.26	8.83
Error ($\mu\text{g m}^{-3}$)	4.91	5.32	4.67	4.89
Fractional Error	0.51	0.47	0.49	0.42
Bias ($\mu\text{g m}^{-3}$)	-4.33	-4.61	-4.01	-3.76
Fractional Bias	-0.43	-0.37	-0.39	-0.27

670
671

672



673

674

675

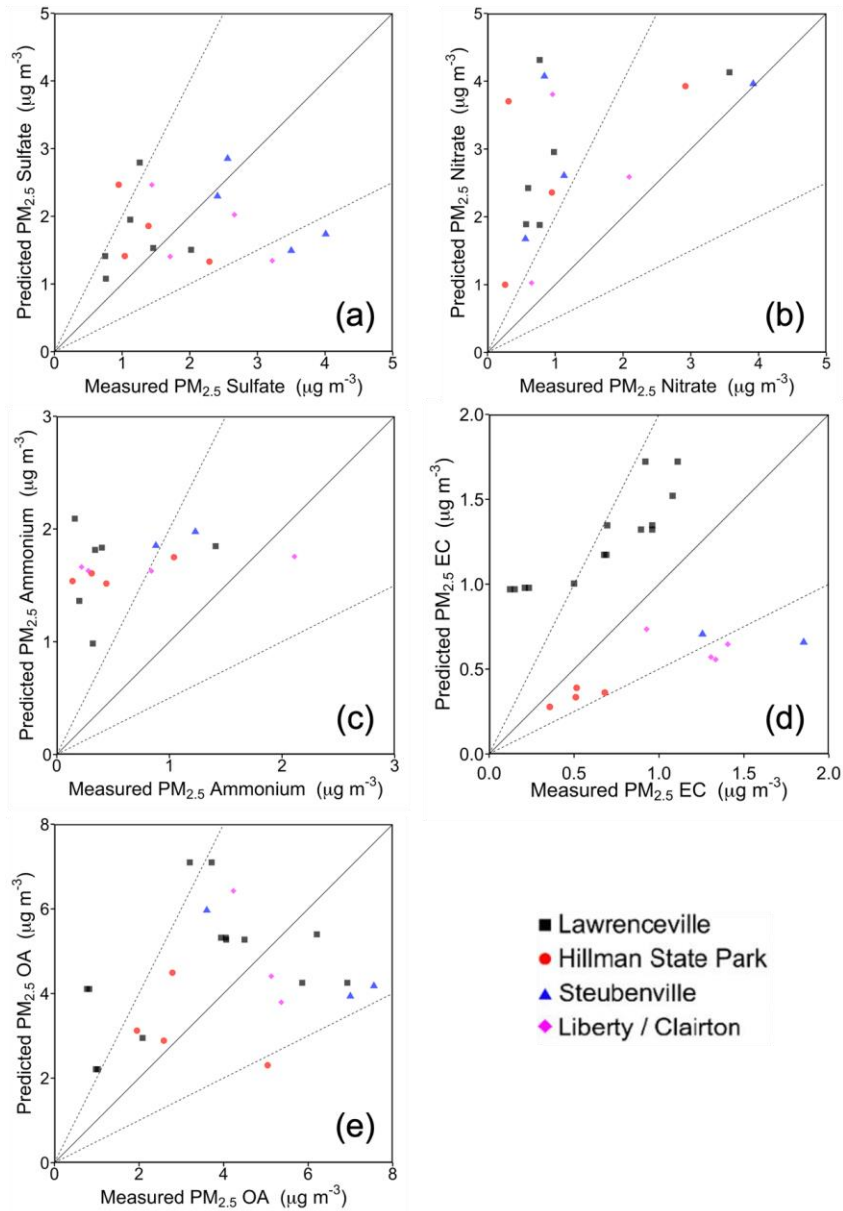
676

677

678

Figure 1. Monitoring sites. (a) Particulate matter speciation measurement sites from EPA-CSN and PM_{2.5} regulatory monitors. The entire inner modeling domain is shown. (b) low-cost sensor sites. City of Pittsburgh boundaries are shown in both panels for reference.

Commented [BD18]: Referee #1 - Comment 5



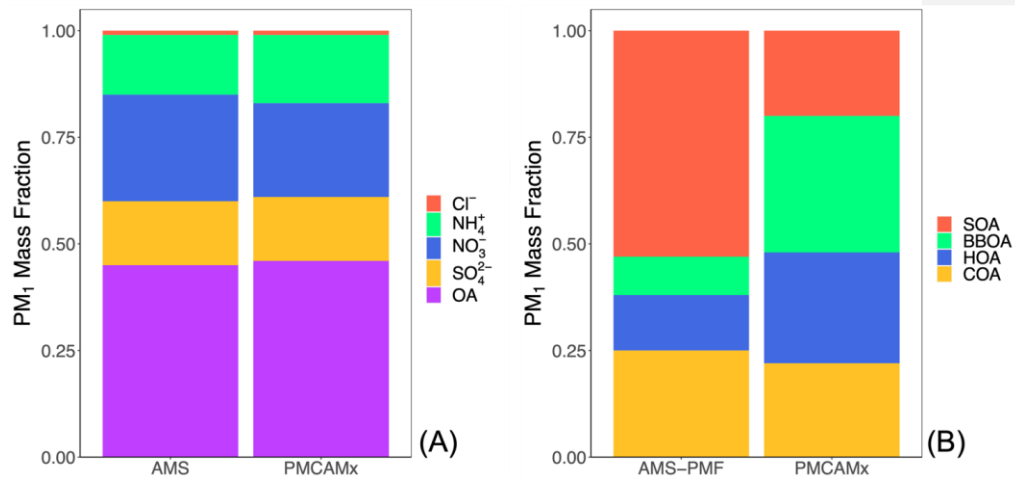
680

681

682

683

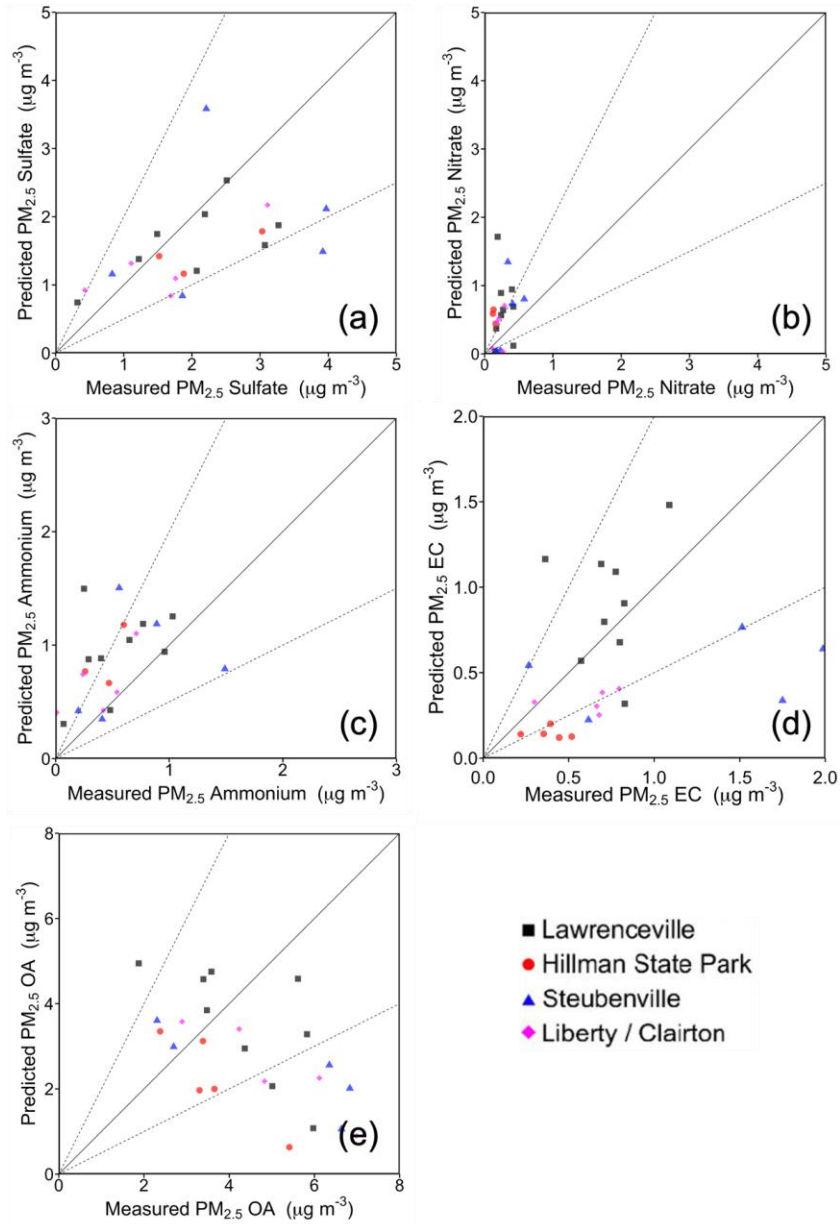
Figure 2. Comparison of daily average PMCAMx-v2.0 predicted concentrations of PM_{2.5} (a) sulfate, (b) nitrate, (c) ammonium, (d) elemental carbon, and (e) organic aerosol with daily measurements from EPA-CSN sites during February 2017.



684
685

686 **Figure 3.** (a) Comparison of PMCAMx-v2.0 predicted composition of PM₁ with the
687 corresponding AMS measurements at the CMU site and (b) organic aerosol composition
688 based on the PMF analysis of the AMS measurements and predicted composition.

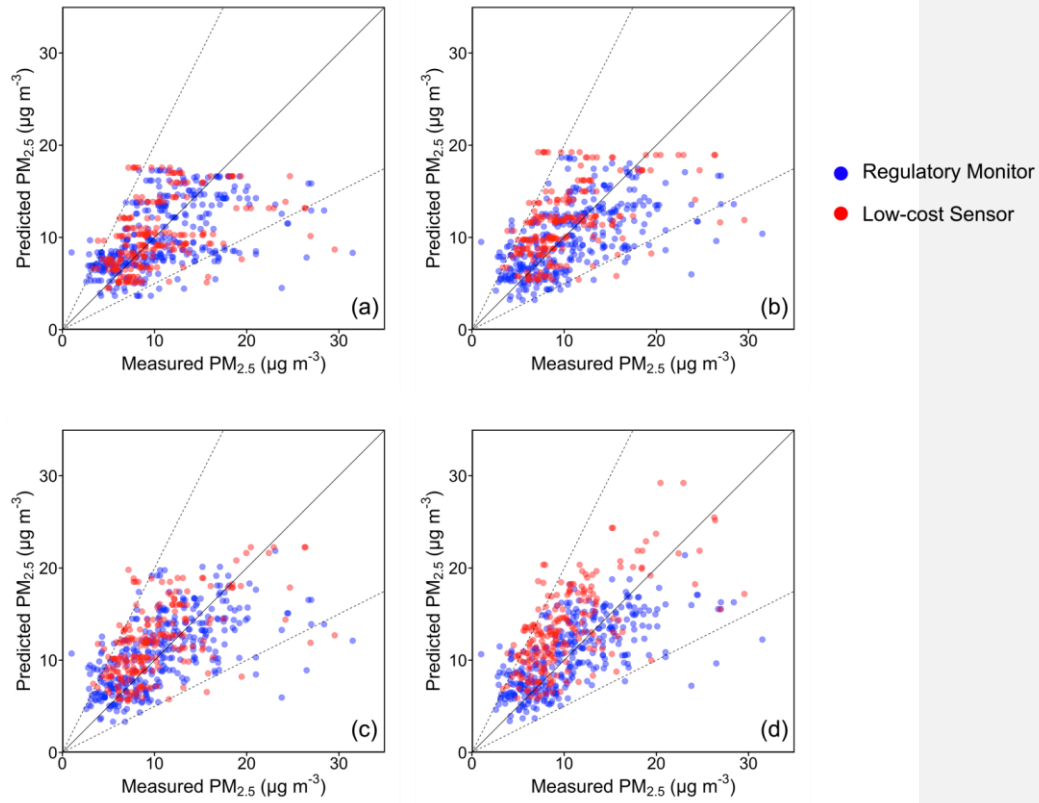
689



690
691
692
693

Figure 4. Comparison of PMCAMx-v2.0 predicted concentrations of PM_{2.5} (a) sulfate, (b) nitrate, (c) ammonium, (d) elemental carbon, and (e) organic aerosol with measurements from EPA-CSN sites during July 2017.

694



695

696

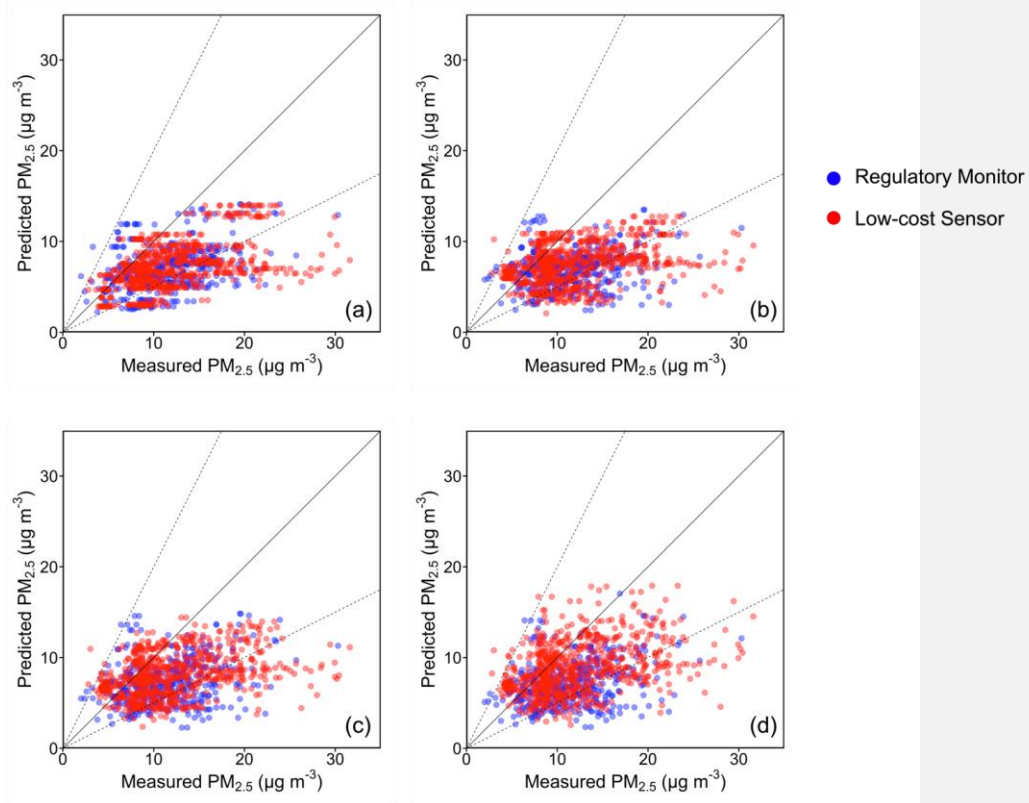
697 **Figure 5.** Comparison of daily average PMCAMx-v2.0 predicted concentrations of PM_{2.5}

698 with daily regulatory measurements and daily low-cost sensor measurements at (a) 36 x

699 36, (b) 12 x 12, (c) 4 x 4, and (d) 1 x 1 km during February 2017.

700

701



702

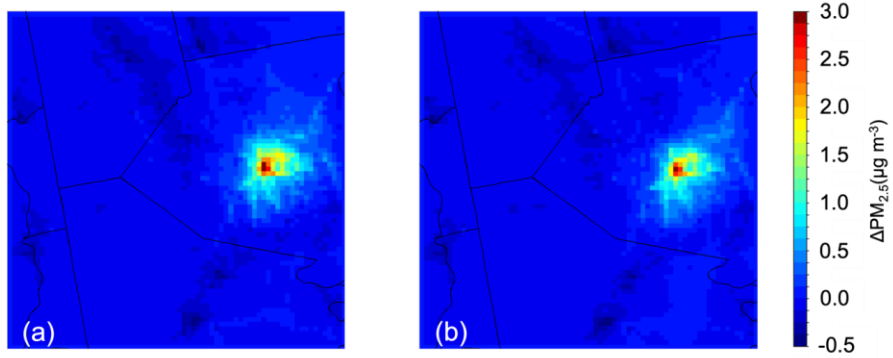
703

704 **Figure 6.** Comparison of daily average PMCAMx-v2.0 predicted concentrations of PM_{2.5}

705 with daily regulatory measurements and daily low-cost sensor measurements at (a) 36 x

706 36, (b) 12 x 12, (c) 4 x 4, and (d) 1 x 1 km during July 2017.

707



708
709
710
711
712
713

Figure 7. Difference between predicted monthly average $PM_{2.5}$ mass concentration when using novel surrogates and original surrogates in (a) February 2017 and (b) July 2017 for the 1 x 1 km resolution simulation grid. A positive value indicates a higher concentration predicted with the novel surrogates.